



저작자표시-비영리-변경금지 2.0 대한민국

이용자는 아래의 조건을 따르는 경우에 한하여 자유롭게

- 이 저작물을 복제, 배포, 전송, 전시, 공연 및 방송할 수 있습니다.

다음과 같은 조건을 따라야 합니다:



저작자표시. 귀하는 원저작자를 표시하여야 합니다.



비영리. 귀하는 이 저작물을 영리 목적으로 이용할 수 없습니다.



변경금지. 귀하는 이 저작물을 개작, 변형 또는 가공할 수 없습니다.

- 귀하는, 이 저작물의 재이용이나 배포의 경우, 이 저작물에 적용된 이용허락조건을 명확하게 나타내어야 합니다.
- 저작권자로부터 별도의 허가를 받으면 이러한 조건들은 적용되지 않습니다.

저작권법에 따른 이용자의 권리는 위의 내용에 의하여 영향을 받지 않습니다.

이것은 [이용허락규약\(Legal Code\)](#)을 이해하기 쉽게 요약한 것입니다.

[Disclaimer](#)

의학박사 학위논문

폐 오가노이드와 유전자 교정을
이용한 섬모운동이상 모델 구축에
관한 연구

CRISPR/Cas9-mediated Lung Organoid

Modeling of Ciliary Dyskinesia

2023 년 8 월

서울대학교 대학원

의학과 중개의학전공

윤 정 기

폐 오가노이드와 유전자 교정을
이용한 섬모운동이상 모델 구축에
관한 연구

지도 교수 김 종 일

이 논문을 의학박사 학위논문으로 제출함
2023 년 4 월

서울대학교 대학원
의학과 중개의학전공
윤 정 기

윤정기의 의학박사 학위논문을 인준함
2023 년 7 월

위 원 장 정 진 행 (인)

부위원장 김 종 일 (인)

위 원 임 재 준 (인)

위 원 최 형 진 (인)

위 원 방 두 희 (인)

Abstract

CRISPR/Cas9-mediated Lung Organoid Modeling of Ciliary Dyskinesia

Jung-Ki Yoon

Department of Medicine, Translational Medicine

The Graduate School

Seoul National University

Lung is the organ that inhale external air for gas exchange, causing continuous exposure to foreign substances. Therefore, various defense mechanisms that remove them have been developed. Mucociliary clearance is one of the importance defense mechanisms to remove relatively large particles deposited on airway. The synchronized motion of cilia on apical side of ciliated cells on airway plays a key role on this mechanism. When genes involved in cilia composition or assembly have defects, primary ciliary dyskinesia (PCD) occurs. The acquired dyskinesia can also occur when ciliary movement decreases due to chronic inflammation or repeated infections. However, research on ciliary movement is limited, and genomic studies using genetic perturbation have been conducted only with animal models, primarily due to the fact that ciliated cells are fully differentiated cells, so that it cannot be studied using cell lines. Primary cell cultures, which cannot be cultured long-term, are also not suitable for gene editing study. In addition, there have been difficulties in measuring ciliary beating frequency (CBF) using the

conventional methods since cilia move together and images of cilia can be easily overlapped for each other.

To address these issues, during this doctoral program, (1) lung organoids that can be cultured long-term were established using patient samples, and it was confirmed that ciliated cells were induced well enough. (2) A novel CBF measurement technique was jointly developed to evaluate the spatial distribution of ciliary movement in the organoids quickly and accurately. (3) The variant with unknown significance discovered through whole-exome sequencing of a PCD family was introduced in normal airway organoids and it is confirmed that the variant causes ciliary dyskinesia.

Through this study, the CRISPR/Cas9-mediated organoid model was established, enabling functional validation of various PCD-causing variants and laying the foundation for future correction through editing, as well as demonstrating the potential for extension to acquired dyskinesia.

**Keywords : Ciliary Dyskinesia, Lung Organoid, CRISPR/Cas9,
Disease Model, Gene Editing**

Student Number : 2020-38357

Contents

Chapter 1. Introduction.....	1
Chapter 2. Materials and Methods.....	11
1. Lung Organoids from Bronchoscopic Brushing Specimens ..	11
2. Immunofluorescent Staining of Organoids.....	12
3. Transmission Electron Microscopy	13
4. Single Cell RNA Sequencing of Lung Organoids	14
5. CRISPR/Cas9 Gene Editing of Lung Organoids	15
6. Ciliary Beating Frequency Measurement of Organoids	16
7. Whole Genome Sequencing of PCD Family	18
Chapter 3. Results	19
1. Motion-contrast based CBF Measurement	19
2. Candidate Gene Selection from a PCD Family	24
3. Lung Airway Organoid from Bronchoscopic Specimens.....	28
4. CRISPR/Cas9-mediated Lung Organoids Modeling of PCD..	31
Chapter 4. Discussion.....	35
Chapter 5. Conclusion and Perspectives	37
References	39
Abstract (Korean)	43

Tables

[Table 3-1]	25
[Table 3-2]	28

Figures

[Figure 1-1]	1
[Figure 1-2]	2
[Figure 1-3]	3
[Figure 1-4]	4
[Figure 1-5]	5
[Figure 1-6]	6
[Figure 1-7]	8
[Figure 1-8]	9
[Figure 3-1]	20
[Figure 3-2]	21
[Figure 3-3]	22
[Figure 3-4]	23
[Figure 3-5]	26
[Figure 3-6]	29
[Figure 3-7]	30
[Figure 3-8]	32
[Figure 3-9]	33
[Figure 3-10]	34

Chapter 1. Introduction

Although the lungs have various functions, such as metabolizing some substances, filtering unwanted materials from the blood, and acting as a reservoir for blood, their most essential function is gas exchange¹. The respiratory system can be divided into two main parts: the airway and the alveolus. The alveolus, where actual gas exchange takes place, is composed of alveolar epithelial cells attached to vessels. The airway, on the other hand, serves as a conduit to transport the inhaled air to the alveoli. (Figure 1-1)

Humans inhale an average of 6 liters of air per minute, and during this process, inhaled particles such as dust and bacteria inevitably breathe together. To counter the threat of inflammation

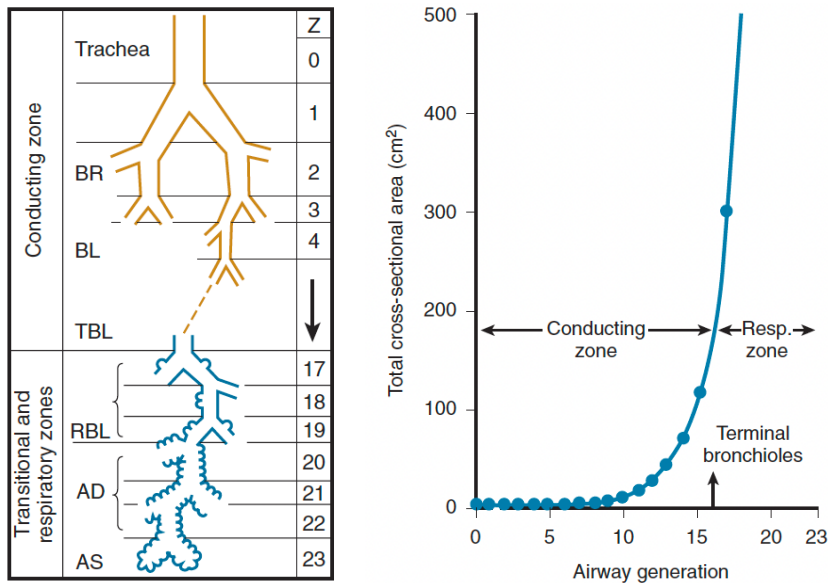


Figure 1-1. Idealization of human lung and total cross-sectional area^{1,2}
 AD, alveolar duct; AS, alveolar sac; BL, bronchiole; BR, bronchus; RBL, respiratory bronchiole; TBL, terminal bronchiole; Z, airway generation

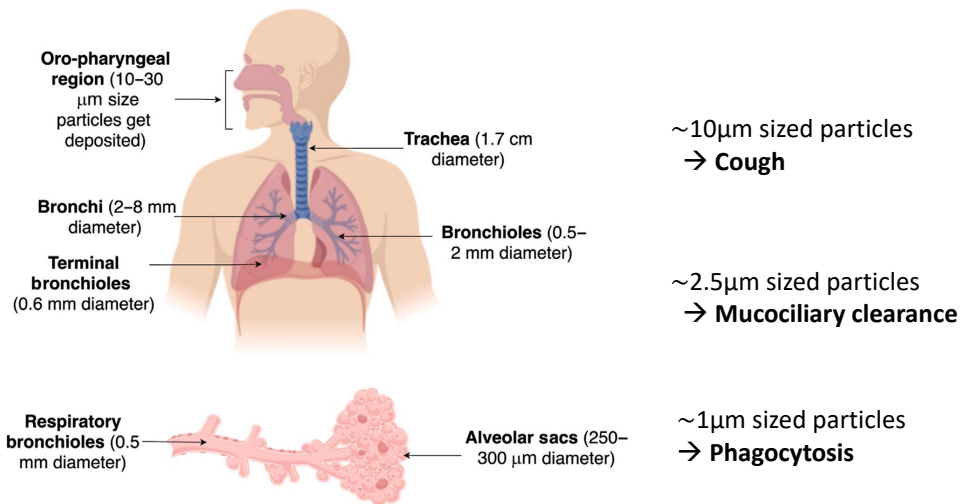


Figure 1-2 Respiratory defense system and the size of inhaled particles ³

and infection, lung have evolved three different defense mechanisms: cough, mucociliary clearance, and phagocytosis.

As the airway branches, the total cross-sectional area expands rapidly, considering continuity equation, leading to a significant reduction in the flow rate of the inhaled air. (Figure 1-1)

$$\text{Continuity equation; } Q = A_1V_1 = A_2V_2 \quad [1]$$

where flow Q , area A , flow rate V

As a result, relatively large particles are deposited in the upper airway and smaller particles can penetrate deeper.^{1,4} (Figure 1-2). Lambert *et al.* built a computed tomography (CT)-based human airway model to assess regional deposition of particles and showed that the particles with diameter ~ 30 microns mainly deposited at oro-pharyngeal regions, whereas the particles with diameter 2.5 microns, called PM2.5, can deposit in deeper regions.⁵

According to major deposit regions, different mechanisms work. First, the largest particles deposited in the oro-pharyngeal are removed by the nasal hairs or expelled by triggering the cough reflex. Secondly, PM_{2.5} reached the alveoli are mainly removed by active phagocytosis of alveolar macrophages. Finally, the particle with diameter 10 microns, called PM₁₀, deposited in the airway, are pushed out through mucociliary clearance.⁶ (Figure 1-2) Mucociliary clearance is consisted of mucus layer and cilia. (Figure 1-3A) Numerous numbers of cilia are lining under mucus layer and propelling mucus as well as substances trapped within the mucus to the pharynx where they will be swallowed.^{7,8}

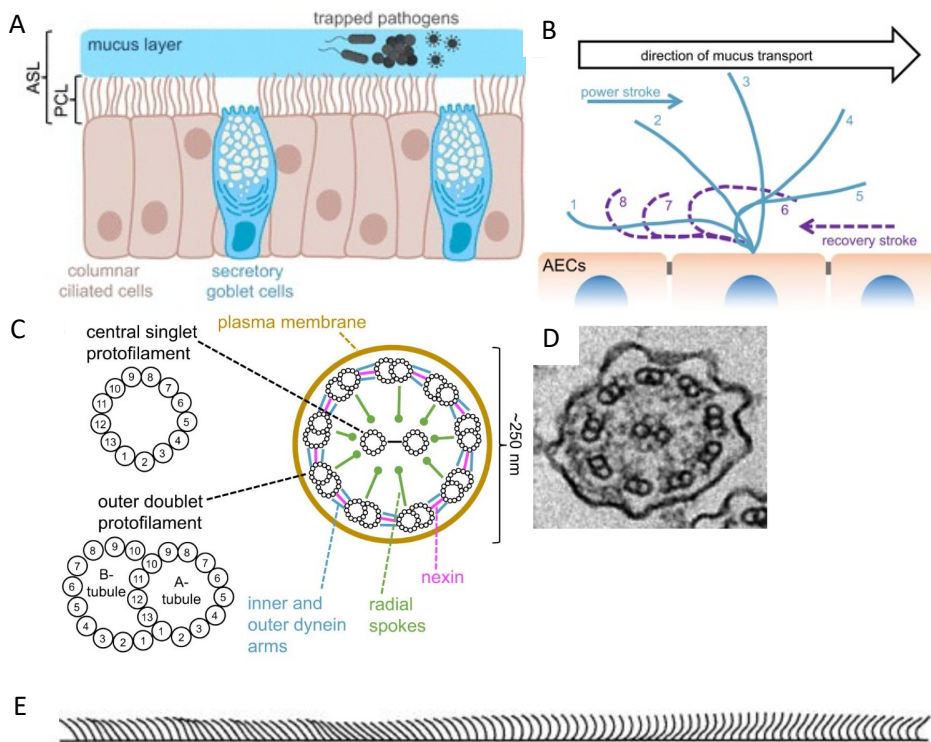


Figure 1-3. Structure and motion of mucociliary system (A) structure of mucociliary clearance (B) motion of cilium (C) cross-sectional structure of cilium and annotations of components (D) electron microscopy image of single cilium (E) metachronal wave of cilia

Motile cilium is a microtubule-based hair-like organelles that line the apical side of epithelial cells lining the respiratory tract including the middle ear and the sinuses, the ductuli efferentes of males, the Fallopian tubes of females, and the ependyma of the brain. Human lung airways are densely covered by cilia, with an estimated count of 10^9 cilia per cm^2 . Each cilium measures approximately $6 \mu\text{m}$ in length and 250 nm in diameter.⁹ The axoneme, the cilia's inner cytoskeletal structure, has a distinctive $9 + 2$ microtubule arrangement and contains important microtubular-associated proteins. (Figure 1-3C,D) Some of these proteins can be visualized through electron microscopy and they include outer and inner dynein arms, radial spokes that link the inner microtubules to the outer ones, and nexin links that connect the outer microtubules to each other. Dynein arms are known to play a vital role in ciliary movement generated by ATP hydrolysis.¹⁰ (Figure 1-4)

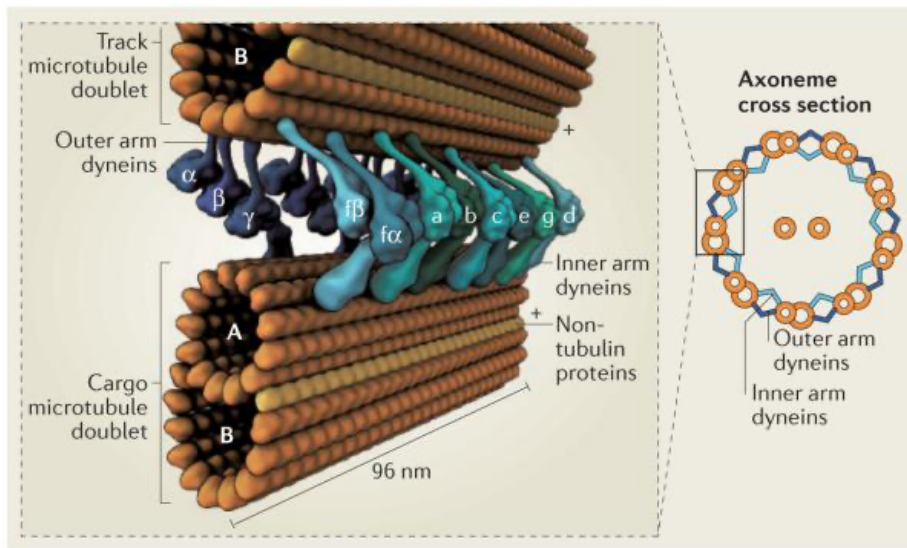


Figure 1-4. Functions of dynein in the axoneme ¹⁰

The movement of cilia have two phases of periodic motions. (Figure 1-3B) During the effective stroke, they move in a straight rod-like manner, while during the recovery stroke, they bend and roll in a mostly tangential direction, bringing them closer to the cell surface. After the recovery stroke, cilia return to a resting position in preparation for the next beat cycle.¹¹ The movement of cilia occurs in a partially synchronized manner with a slight time lag among neighboring cilia, resulting in a metachronal wave. (Figure 1-3E)

Defective cilia called ciliopathies can be caused by genetic disorders such as primary ciliary dyskinesia (PCD).¹² PCD is a rare autosomal recessive inherited disease characterized as respiratory distress newborn, chronic rhinitis, chronic cough, and lateral defects.^{13,14} Since cilia are composed of multiple components, more than 40 PCD causing have been reported, standing for genetic heterogeneity.¹⁵ (Figure 1-5) In addition, multiple PCD-causing mutations have been reported in each PCD-causing gene, making it more difficult to assess the functions of variants and limiting the role of transitional disease models such as transgenic models.¹⁶

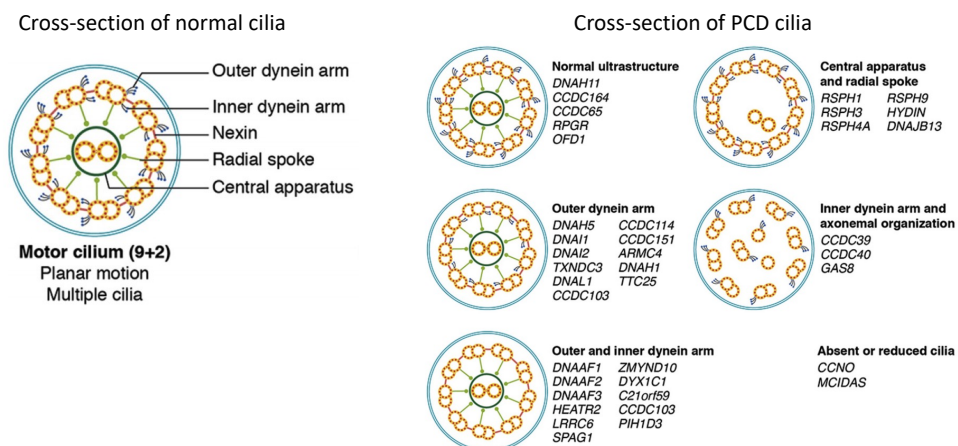


Figure 1-5. Cross-sectional ultrastructure of normal and PCD cilia with affected genes¹⁶

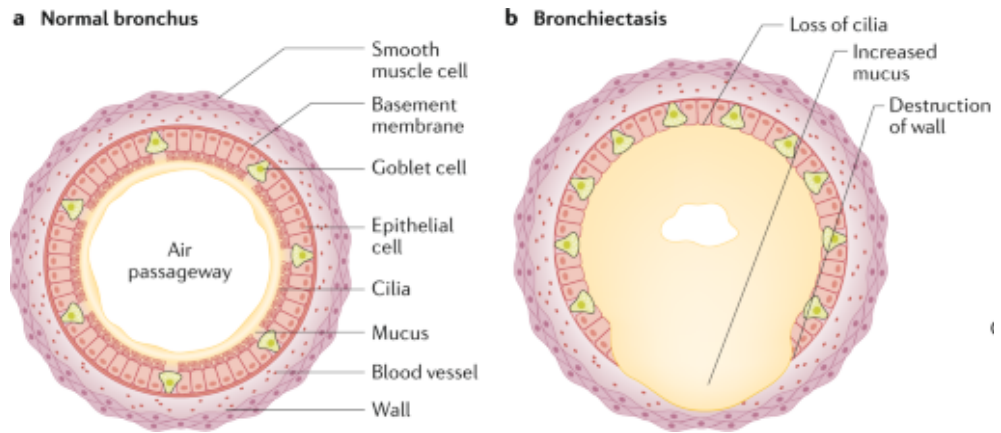


Figure 1-6. Mucociliary defects in bronchiectasis¹⁷

Ciliary dysfunction is not only caused by inherited diseases, but is also common in chronic lung diseases, such as chronic obstructive pulmonary disease (COPD), bronchiectasis, and chronic infections.^{17,18} (Figure 1-6) Chronic inflammatory states can cause constitutive damage to epithelial cells, resulting in abnormal ciliary movement.¹⁹ In addition, mucociliary dysfunction itself can cause mucus thickening and muco-obstruction.²⁰ This obstructive state reduces ciliary movement, creating a vicious cycle, and can lead to recurrent pneumonia and the progressive destruction of lung architecture. Therefore, analyzing and modeling the motion of respiratory cilia is often employed to investigate the pathophysiology of lung diseases.

Nonetheless, modeling cilia poses several challenging issues. Firstly, cell-based models for cilia are limited, especially since ciliated cells are fully differentiated and do not divide, making it impossible to create a long-term cell line. The primary cell culture with an air-liquid interface (ALI) is widely used, but it is not suitable for genetic perturbation due to its limitations in long-term culture and expansion. Secondly, imaging ciliary motion is difficult. Cilia

move rapidly (normal range of frequencies, 10–14 Hz), and two distinct patterns of stroke easily cause out-of-focus images. The overlapping of cilia in images with surrounding cilia moving in bundles can interfere with the measurement of ciliary beating frequency (CBF). Thirdly, genetic mutations that cause PCD are diverse, with different variants being reported within each gene. Therefore, it can be difficult to determine whether an individual's identified genetic mutation is responsible for causing ciliopathy.

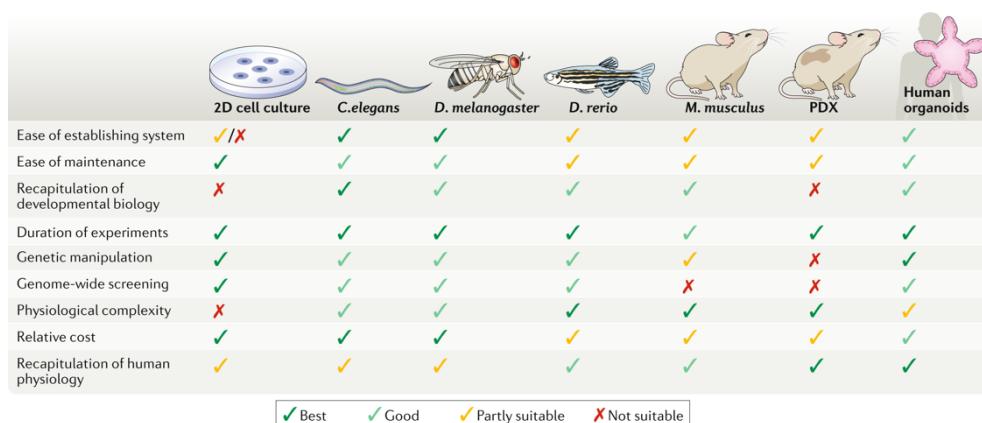
Historically, scientists have developed and employed various disease modeling systems to understand the molecular and cellular mechanisms as well as physiological functions of organs. The classical models such as primary cell cultures, immortalized cell lines, and animal model systems have uncovered the mechanisms of disease, or found clues for treatment, but have also revealed clear limitations in many areas.²¹

Primary cell culture refers to a two-dimensional (2D) culture system in which patient cells are cultured, characterized, manipulated over short periods of time. This approach offers the advantage of preserving patient-specific characteristics and fully differentiated cells such as ciliated cells in lung.²² However, due to the constraints on long-term cultures, primary cell cultures present significant challenges for gene editing using CRISPR/Cas9. Therefore, it is not well-suited for studying ciliopathies through genetic perturbation.

Immortalized cell line represents a 2D system where patient cells are rendered infinitely proliferative through immortalization techniques and subsequently cultured over extended durations. Unlike primary

cell cultures, immortalized cell lines enable long-term culture, facilitating gene editing procedures. However, cell lines lack fully differentiated cells and frequently undergo alterations in patient or organ characteristics during the immortalization process²³ or contamination with other cells²⁴, making them unsuitable for studying differentiated cells such as ciliated cells.

Animal models involve the use of various animals with organs or cellular organelles that exhibit similarities to those of humans. Transgenic models, in particular, can be employed for diverse purposes such as lineage tracing and visualization of cellular activity under specific conditions.²¹ Nevertheless, disparities between animal and human characteristics limit the direct application of findings from animal studies. Additionally, studying multiple gene perturbations poses challenges as generating transgenic mice requires substantial time, effort, and subsequent aging to the desired stage.



The table compares seven model systems across ten criteria. The systems are 2D cell culture, C. elegans, D. melanogaster, D. rerio, M. musculus, PDX, and Human organoids. The criteria are: Ease of establishing system, Ease of maintenance, Recapitulation of developmental biology, Duration of experiments, Genetic manipulation, Genome-wide screening, Physiological complexity, Relative cost, and Recapitulation of human physiology. A legend indicates: Best (green check), Good (green check), Partly suitable (yellow check), and Not suitable (red X).

	2D cell culture	C. elegans	D. melanogaster	D. rerio	M. musculus	PDX	Human organoids
Ease of establishing system	✓/✗	✓	✓	✓	✓	✓	✓
Ease of maintenance	✓	✓	✓	✓	✓	✓	✓
Recapitulation of developmental biology	✗	✓	✓	✓	✓	✗	✓
Duration of experiments	✓	✓	✓	✓	✓	✓	✓
Genetic manipulation	✓	✓	✓	✓	✓	✗	✓
Genome-wide screening	✓	✓	✓	✓	✗	✗	✓
Physiological complexity	✗	✓	✓	✓	✓	✓	✓
Relative cost	✓	✓	✓	✓	✓	✓	✓
Recapitulation of human physiology	✓	✓	✓	✓	✓	✓	✓

Figure 1-7. Comparison of model systems²¹

Organoids are self-organized three-dimensional in vitro tissue cultures consisted of adult epithelial stem cells and their differentiated cells, which mimic their corresponding *in vivo* organ.²⁵⁻

Recently, the niches required for proliferation and differentiation of lung airway cell types^{29,30} and alveolar cell types^{31,32} have been identified. Accordingly, long-term organoid culture of both airway and alveolar stem cells are possible. Organoid enable us to culture patient-derived cells for a long time and can generate fully differentiated cells from maintaining stem cells. Owing to this, it is now possible to study cilia through direct genetic perturbation of human cells without the use of animal models, and to create long-term organoid models with genetic disorders, offering new opportunities for studying the pathophysiology of lung diseases. The combination of organoid and gene editing technologies has been revolutionized on a range of fields³³⁻³⁶ This advancement in organoid culture methods is a significant step towards improving our understanding of the mechanisms underlying ciliary dysfunction and its role in lung disease.³⁷

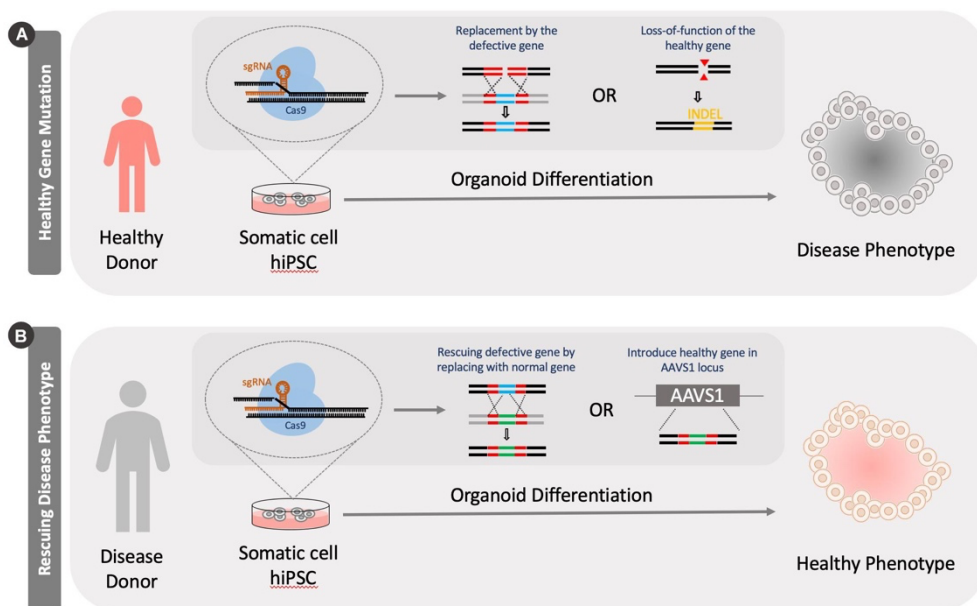


Figure 1-8. Generation of disease models using CRISPR/Cas9 tools³⁸

In this study, lung airway organoids were established from respiratory samples obtained through various methods. Also, a new method measuring CBF was developed to overcome issues encountered. Using this approach, the function of variants of unknown significance found in primary ciliary dyskinesia (PCD) patients was validated through CRISPR/Cas9-mediated lung organoid and subsequent CBF measurements.

Chapter 2. Materials and Methods

1. Lung Organoids from Bronchoscopic Brushing Specimens

The patients who were supposed to receive bronchoscopy for clinical needs were enrolled and informed consents were obtained. Collection and use of human specimens were reviewed and approved by the institutional review board of Seoul National University Hospital [1602-108-742]. On bronchoscopy, the normal lesions of right middle bronchus were brushed and delivered in Advanced DMEM/F12 (Gibco, USA) with Glutamax (Gibco), HEPES (Gibco), Penicillin-Streptomycin (Gibco), named AdDF+++ hereafter. Brushing specimen was centrifuged at 400 g for 5 min at 4°C and the pellet was resuspended in AdDF+++ with amphotericin B and 1mg/mL collagenase IV (Sigma-Aldrich), followed by digestion for 15 min at 37°C. After filtration using a 70-µm filter, the suspension was centrifuged at 400g for 5 min at 4°C with 10mL of AdDF+++. The pellet was resuspended in 1mL of 1x Red Blood Cell Lysis Solution (Miltenyi Biotec, USA) for 10 min at room temperature, followed by addition of AdDF+++ and centrifugation. The pellet was seeded in Matrigel GFR (Corning, USA), solidified for 15 min at 37°C, and cultured in lung airway organoid media ²⁹. The media was changed every 2~3 days and the organoids were subcultured every 2~3 weeks depending on the density and growth dates of organoids.

Once the organoids were stably maintained, air-liquid interface (ALI) culture was used to facilitate differentiation of basal cells to

ciliated cells. The dissociated organoids (1×10^6 /mL) were placed at the apical insert of 0.4 μm pore sized Transwell (Corning) and cultured in lung airway organoid media. When the confluence reached >70% of the insert, the media placed only at the basolateral chamber and started ALI culture. CBF of ciliated cells was measured at least after 28 days of ALI culture.

2. Immunofluorescent Staining of Organoids

Matrigel was dissolved with ice-cold Cell Recovery Solution (Corning) at 60 rpm for 30 to 60 mins at 4°C on horizontal shaker (CRYSTE). The recovered organoids were fixed in 4% paraformaldehyde for 30 min at 4°C. The samples were then washed with 0.1% TritonX-100/PBS (PBS-T). They were next permeabilized in 0.2% Triton X-100/PBS for 5 min and incubated in 5% donkey serum (Jackson ImmunoResearch)/PBS-T blocking solution for 2 hours at RT. Primary antibodies were incubated for overnight at 4°C at the indicated dilutions: Chicken-anti-CK5 (1:500, Biolegend, 905904), Rabbit-anti-Acetyl- α -Tubulin (1:200, Cell Signaling Technology, 5335), Phalloidin-488 (1:500, Abcam, ab176753). Alexa Fluor-coupled secondary antibodies (1:500, Invitrogen) were incubated for overnight at 4°C. After antibody staining, nuclei were stained with DAPI (1:1000, Sigma) and sections were embedded in Vectashield Plus antifade mounting medium (H-1900, Vector laboratories). Fluorescence images were acquired using either Leica SP8 or LSM700 confocal microscopes. LAS X (Leica) or ZEN software (Zeiss) was used for processing fluorescent images.

3. Transmission Electron Microscopy

Fully differentiated lung organoid was washed with 200 μ L of PBS for 5min at room temperature (RT), fixed with a mixture of cold 2.5% glutaraldehyde in 0.1 M phosphate buffer (pH 7.2), and 2% paraformaldehyde in 0.1 M phosphate (pH 7.2) overnight at 4°C, followed by additional fixation with 2% osmium tetroxide in 0.1 M phosphate buffer for 1.5 hours at RT. Fixed organoid was washed briefly with 0.1 M phosphate buffer, was dehydrated throughout a graded 50, 60, 70, 80, 90, 95, 100%, 100% ethanol series, was infiltrated by using propylene oxide and EPON epoxy resin mixed (Embed 812, Nadic methyl anhydride, poly Bed 812, dodecenylsuccinic anhydride, dimethylaminomethyl phenol; Electron Microscopy Polysciences, (USA), and then finally was embed with only epoxy resin. Polymerization was done in capsules at 80°C for overnight. The samples were cut on ultramicrotome (RMC MT-XL) at 65 nm and stained with saturated 4% uranyl acetate and 4% lead citrate. TEM images were obtained at 80 Kv with a transmission electron microscope (JEM-1400; Japan) in Department of Research & Experiment at Seoul National University Hospital.

4. Single Cell RNA Sequencing of Organoids

Organoids were dissociated into single cells and resuspended in 1 ml of ADF+++ and filtered using a 30 μm SmartStrainer (Miltenyi Biotec). Samples were analyzed using ReadyCount Green/Red Viability Stain (Invitrogen) for counting the number of cells and measuring cell viability with automated cell counter Countess 3 FL (Thermo Fisher) and centrifuged at 400 g for 5 min at 4°C, and then resuspended in 0.04% bovine serum albumin (BSA) solution at appropriate volume for loaded on Chromium Next GEM microfluidic chip and processed as manufacturer's protocol. All libraries were sequenced in NovaSeq 6000 system (Illumina) in paired-end mode.

Raw sequencing data were aligned to GRCh38 human reference genome with Cell Ranger (v6.0.1).³⁹ Ambient RNA were removed by using CellBender (v0.2.1)⁴⁰ to remove background noise expression and doublets. Only cells assigned a single donor, passed doublet filter, express more than 200 genes, and not express more than 10% mitochondrial genes are used to further analysis. SCTransformation in Seurat package (v4.0.3)⁴¹ regressing out mitochondrial gene percentage (percent.mt) was done for normalization. Batch effect between sequencing libraries was corrected by using canonical correlation analysis (CCA) with up to 50 PCs as integration method. RunPCA, RunUMAP, and FindNeighbors followed by FindClusters with Louvain algorithm in Seurat package were accomplished to visualize UMAP plot and cluster cells.

5. CRISPR/Cas9 Gene Editing of Lung Organoids

Four lentiviruses were produced by using Lipofectamine 3000 (ThermoFisher Scientific) as the manufacturer's protocol: LentiCas9-Blast (Addgene #52962) and lentiGuide-Puro (Addgene #52963) with 3 different sgRNA sequences. These sgRNA were designed by CRISPOR⁴² to introduce indels around 339th amino acids of DYX1C1.

sgRNA#1: 5'-AAATATATCCTTCTATTAAT-3'

sgRNA#2: 5'-GGATATCTATGTATGATATA-3'

sgRNA#3: 5'-GGCTATTGAAGATTCTTCTA-3'

Established organoids were mixed with the lentivirus product of lentiCas9-Blast, centrifuged at 400g for 60min at 32°C (spinoculation), incubated for 6 hours at 37°C in CO₂ incubator, and then performed blasticidin selection under airway organoid media for 2 weeks. The SpCas9 transfected organoids were further infected by the lentivirus product of lentiGuide-Puro with the guide sequence as the same protocol to lentiCas9-Blast, followed by puromycin selection for 2 weeks. T7 Endonuclease I (catalog #M0302S, NEB, USA) was used for T7EI assay. PCR amplification and Sanger sequencing was performed with primers listed below:

Forward primer: 5'- CCGGCCAGTAACAGCTGATT-3'

Reverse primer: 5'- TGCAACGGAAAAC TATTTGGCA-3'

6. Ciliary Beating Frequency Measurement of Organoids

A home-built bright-field optical microscope were developed by Dr. Woo June Choi⁴³ and established in Joongang University. A 150 W halogen lamp (OSL2, Thorlabs, USA) was coupled with a Köhler illumination setup for lighting. Light rays ($\lambda_0 = 600$ nm) were directed onto an organoid sample via a non-polarized beam splitter (BS) and a 25 \times water dipping objective lens (N25X-APO-MP, 1.1 N.A., 2.0 mm W.D., Nikon, Japan). Light reflected from the sample was collected via the objective and the BS, and focused through a 0.75 \times infinity-corrected tube lens ($f = 200$ mm) onto a high-speed CMOS camera (VC-2MC-M340, 337.6 fps for free-run mode, 5.5 μm^2 pixel size, Viewworks, Korea) capturing 8-bit gray-scaled images (2048 pixels \times 1088 pixels) at 200 to 300 fps over a medium configuration Camera Link connection. The temperature of the organoid culture was controlled by a closed-loop thermistor plate (TLK-H, Thorlabs, NJ, USA).

The captured images were contrast-enhanced in batches to improve viewing and then registered. Image registration was performed with a function custom-written in MATLAB, by which each image was automatically aligned with a reference image (the first frame) by estimating the geometric translation transformation. Therefore, possible slow drift and mechanical motion artifacts in the recording that might interfere with ciliary motion signals were pre-corrected.

To identify the cilia in the images, Eigen-decomposition (ED)

filtering⁴⁴ was applied to the registered images. ED filtering is an adaptive clutter rejection technique that utilizes statistical properties of time-varying signals and effectively extracts ciliary motions from the static background. Thus, ED filtering generated a motion-contrast image, which improved localization of the cilia in the organoids. The motion-contrast image was observed, and a ROI involving the individual cilia was selected. Further, cross-correlation was performed with the ROI images, and we measured the similarity between the first frame (a reference frame) and the rest of the frames to determine the oscillatory correlation coefficients. Smoothing was taken to the correlation coefficients using a low-order polynomial fitting to remove possible spurious spikes on the profile. The peaks of the resulting coefficient waveform were counted, and the counts were divided by the recording period (total frames/frame rates), which represented the CBF for the cilia in the ROI.

7. Whole Genome Sequencing of a PCD Family

Two PCD affected siblings and their normal parents were enrolled in whole-genome sequencing (WGS) study for familial bronchiectasis at Seoul National University Hospital (NCT03809091) and informed consents were obtained (IRB number 1812-105-995). Whole blood (5mL) was collected in EDTA tubes from each participant and DNA was extracted by using DNeasy Blood & Tissue Kit (Qiagen, USA). Whole genome sequencing library construction and sequencing were performed by Macrogen (South Korea). Raw data was aligned to GRCh38 human reference genome by using bwa⁴⁵ with default parameters. Single nucleotide polymorphisms (SNPs) and short indels were called by GATK HaplotypeCaller.⁴⁶ Variants were annotated by ANNOVAR.⁴⁷ Non-coding, nonsynonymous, common variants (MAF > 1% in 1000 Genome Project) were excluded.

Chapter 3. Results

1. Motion-contrast based CBF Measurement^①

Initially, the conventional method of single-point Fast Fourier Transform (FFT) analysis technique was used to measure the ciliary beat frequencies (CBFs) of organoids. A total of 200 images of fully differentiated human airway organoids were captured at 200 fps. (Figure 3-1) However, the conventional method produced significant multiple spectral peaks due to interference from the movement of other cilia, making it difficult to determine the fundamental frequency of ciliary motion. For example, in Figure 3-1, CBFs of 9Hz, 19Hz, 28Hz, and 38Hz are possible, but it is impossible to determine which is the actual CBF from these values alone. Considering the normal range of CBFs, which is 10-14Hz, 9Hz corresponds to hypoactive ciliary motion, while 19Hz and others correspond to hyperactive ciliary motion, which are opposite results. Therefore, it is necessary to develop a measurement method that can overcome this signal redundancy.

To solve this problem, first a process that separates fast-moving objects from the background is required. In this study, the motion-contrast imaging technique was utilized. Motion-contrast imaging is an image processing technique that emphasizes the shape or position of moving objects and separates them from a static background. The technique utilizes refraction or scattering caused by differences in

^① A part of this section was published in *IEEE Transactions on Medical Imaging* (2021) doi:10.1109/TMI.2021.3112992

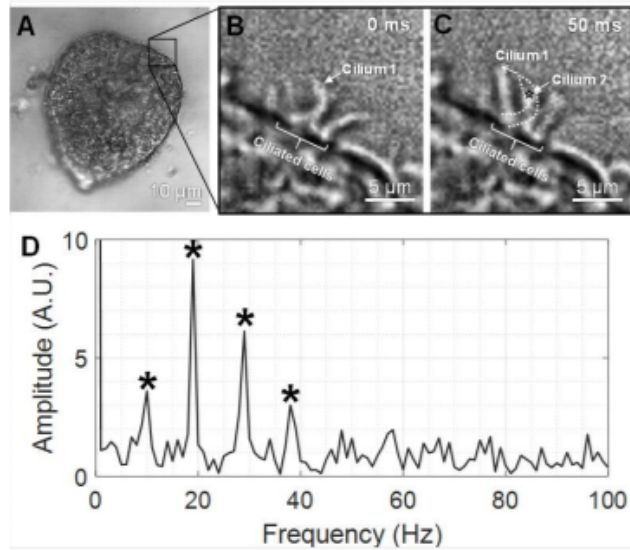


Figure 3-1. Signal redundancy of the conventional single-point fast Fourier transformation (FFT) method (A) Bright-field image of a healthy human airway organoid. (B, C) Magnification of the boxed area with 50ms interval (D) FFT spectrum of a time-course intensity profile recorded at 200 Hz at the position (star) in (C). CBFs were confounded by harmonics (asterisks).

the refractive index of materials surrounding the objects. In other words, because the materials surrounding the objects refract light differently, motion-contrast imaging can separate moving objects from their surrounding background to produce clearer images.

Next, a color-coded motion-contrast image was superimposed onto the bright-field image obtained from the region of interest (ROI), with yellow indicating high cilia motility. (Figure 3-1) The ciliated cells within the ROI were analyzed by calculating the correlation between the ROI frames. The resulting correlation coefficients showed a regular waveform, which was attributed to ciliary motion and allowed for the calculation of the CBF. The CBF calculated using the 200 images previously measured was 9Hz, which was consistent with the manually counted CBF.

Since cilia is a slender, unevenly lined, and micrometer-sized structure with waving motions, it is easily captured out of focus, which make it challenging for users to adjust them within the focal plane. Moreover, cilia in organoids created based on 3D culture are particularly vulnerable to the out-of-focus issue because they are less likely to be in the same plane compared to those in 2D culture.

To evaluate the sensitivity at different optical foci, cilia image stacks were collected twice from the same organoid, one with focused and non-overlapping cilia and the other with out-of-focus

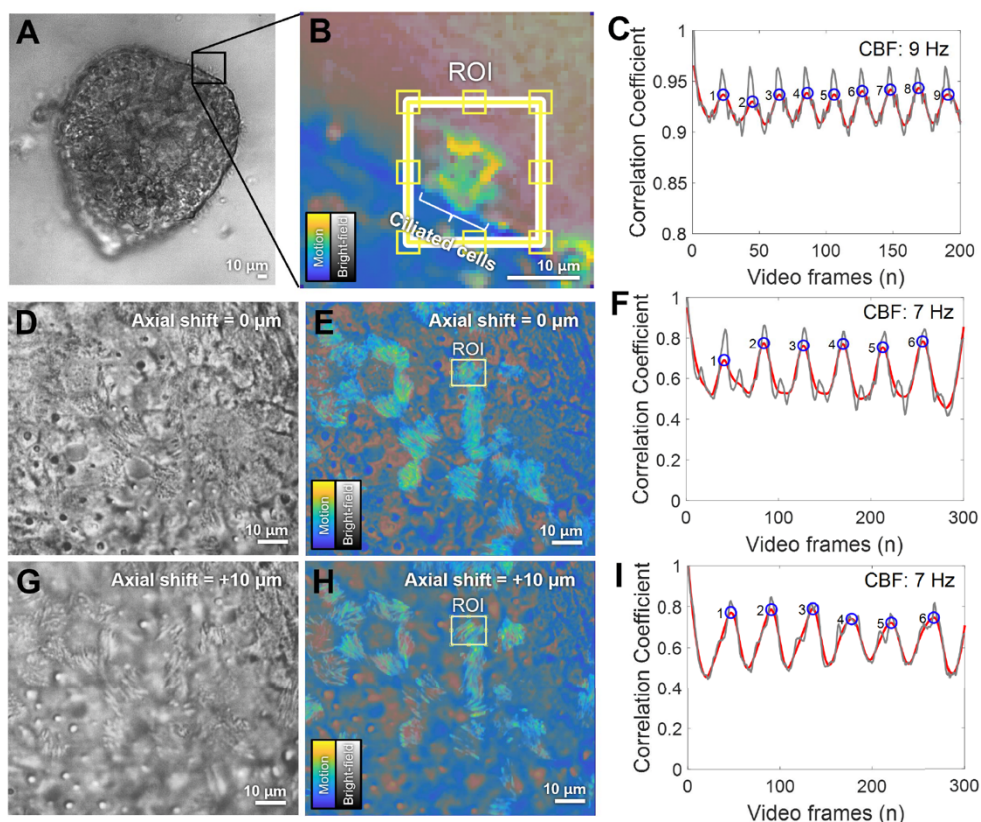


Figure 3-2. Evaluation of the proposed CBF measurement. (A) Bright-field image of a healthy human airway organoid. (B) a motion-contrast image superimposed with bright-field image and an ROI for correlation calculation (C) The correlation coefficients over time. The CBF calculated with counts of peaks in the smoothed profile (red line) over 1s. (D-I) Sensitivity analysis of CBF measurements with axial shifts (10 μm), showing focus-independent estimates of CBF.

cilia collected with a focus on an area that was 10 μm higher. Correlation was performed on identical regions of interest (ROIs). The coefficient profiles differed significantly in the amount of noise, but the CBF estimates were identical in both cases. This showed that the proposed method is robust to focal shifts and can process out-of-focus images.

In contrast to the conventional method, this approach, acquiring a wide area of images, is advantageous for spatial mapping and facilitates the measurement of inter- and intra-organoid CBFs. From multiple ROIs in single organoid, the spatial distribution of CBFs was measured. The CBFs ranged from 5 to 10 Hz (mean: 7, standard

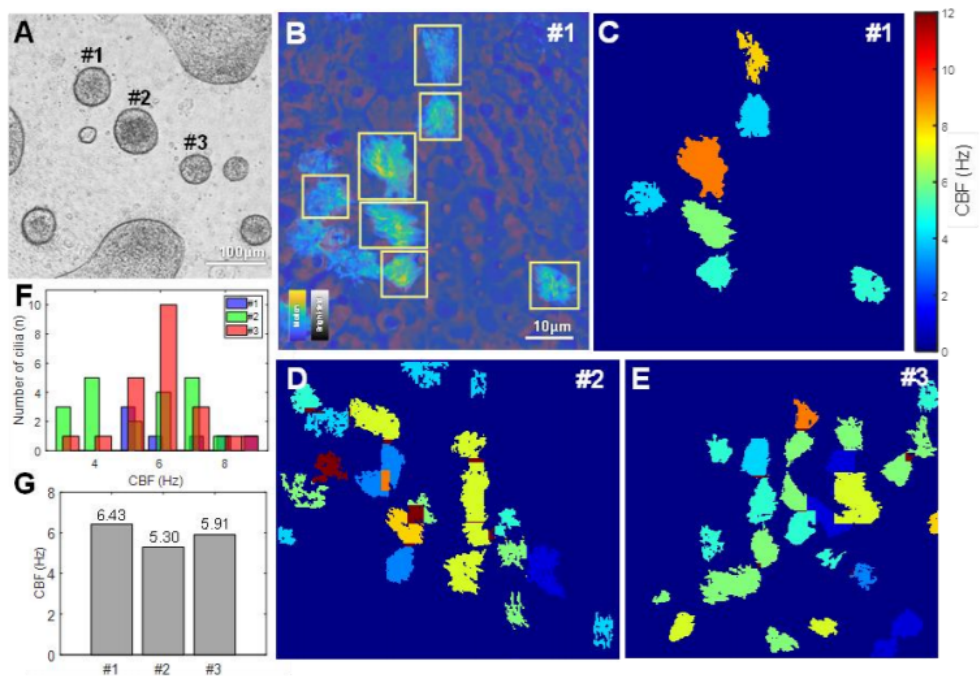


Figure 3-3. Spatial distribution of CBFs. (A) Bright-field image of a healthy human airway organoids (B) Overlaid images of organoid #1 and ROIs for CBF measurement (C, D, E) CBF maps of cilia on organoid #1, #2, and #3. (F) Intra-/inter-organoid variation of CBF. (G) Mean CBF of organoids.

deviation: 1.8) at room temperature and exhibited significant local variance within organoid. Inter-organoids CBFs were also measured from 3 organoids and the average values of CBFs were 6.43, 5.30, and 5.91 Hz, showing minor variations between them.

Both *in vitro* and *in vivo* experiments have shown that CBF varies with temperature. To verify this observation, longitudinal measurements were performed subjected to temperature variations (23–32°C). As expected, the movement of cilia on the organoids and CBF increased swiftly with temperature, with a linear increase in mean CBF from 5.63 to 9.72 Hz, along with an increase in variance and mean values. The CBF values exhibited a slope of 0.5 Hz/°C.

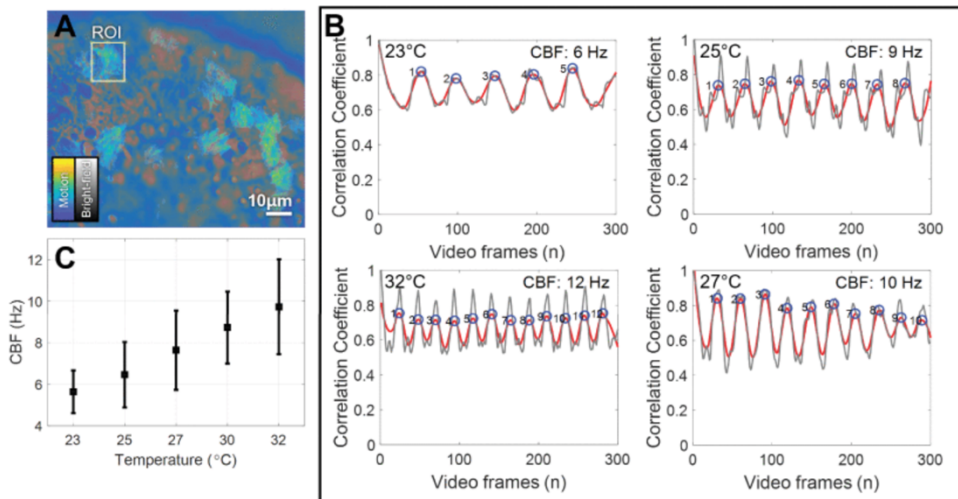


Figure 3-4. Temperature dependence of CBF (A) Motion-contrast image of healthy human airway organoid. (B) Change in CBF correlations with temperature (23–32°C) (C) CBF on temperature for different ROIs from two organoids (number of ROIs = 5)

2. Candidate Gene Selection in a PCD Family

In 2020, two siblings, aged 23 and 28, referred to the pulmonary clinic at Seoul National University Hospital with persistent and recurring non-tuberculous mycobacterium pulmonary disease (NTM-PD). Both siblings reported a long-standing history of frequent pneumonia since childhood while no history of neonatal respiratory distress syndrome was reported. Upon examination, one sibling was diagnosed with situs inversus. Also, both have bronchiectasis with ill-defined nodules in both lungs and bilateral spheroid and ethmoid sinusitis on computed tomography (CT) scans. Other labs including auto-antibody panels and serology were negative. Their parents have no history of pneumonia and sinusitis and normal lungs on CT scan. This family was subsequently enrolled in the whole-genome sequencing (WGS) study for familial bronchiectasis at Seoul National University Hospital (NCT03809091).

Participant's blood-derived DNA was extracted and subjected to whole-genome sequencing (WGS), generating an average of 793M reads (range: 765M – 851M), with a mean depth of 42x (range: 40x – 45x) and an average 20x coverage of 97% (range: 94% – 99%). A total of approximately 4M single nucleotide polymorphisms (SNPs) and 950k small indels were identified. Among the 6,778,293 SNPs/indels identified across the entire family, 39,903 coding variants and 23,503 non-synonymous variants were found. From non-synonymous variants, the common variants found in more than 1% of the total population within the 1000 Genome Project were removed, and 6,326 SNP/indels were retained for further trio analysis. Although the trio analysis was conducted on a single family,

ID	PCD	reads (millions)	mean depth	20x coverage	# SNP	# small indels
01-1-01	affected	851	45x	98%	4,065,978	963,962
01-1-02	affected	773	41x	99%	4,041,443	951,988
01-2-01	not affected	765	40x	94%	4,056,293	952,014
01-2-02	not affected	782	41x	97%	4,043,389	950,834

Table 3-1. Summary of sequencing quality and detected variants

the fact that both siblings exhibited the same phenotype allowed for a reduction in candidate genes by assuming they possessed the same genotype.

Considering the pedigree, three mutation patterns can be possible. First, *de novo* mutations can arise spontaneously in both siblings and be absent in both parents. In this study, this pattern was identified in 4 genes (CACNA1B, CTBP2, MUC6, KRTAP5-7). Second, simple recessive mutations can occur when siblings inherit one copy of the same mutations from both carrier parents. In this study, this pattern was identified in 9 genes (HEATR1, OR2T35, ANKRD36, ATXN1, FOXD4, ENKUR, PDPR, LOC101928710, RBFADN). Lastly, compound heterozygous mutations can occur when both parents carry different variants in the same gene and the siblings each inherit them. This pattern was observed in 5 genes (CSMD1, PRR23D1, DYX1C1, VPS13C, HELZ2).

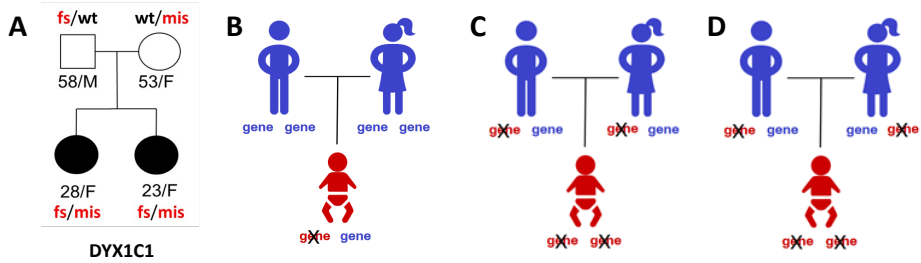


Figure 3-5. Pedigree of a PCD family and possible inherited patterns of variants (A) Pedigree with a candidate gene (B) inherited pattern of de novo mutation (C) inherited pattern of simple recessive mutation (D) inherited pattern of compound heterozygous mutation.

DYX1C1, also known as DAAF4, is a known gene that causes PCD⁴⁸. It encodes an outer dynein arm assembly factor that forms a crucial component of the cilia's ultrastructure. The gene contains two functional domains, CS domain and tetratricopeptide repeat (TPR) domain. Three consecutive TPR domain were located at N-terminus and interacts with chaperones such as HSP90 to facilitate cilia assembly⁴⁹. Both *Dyx1c1*^{Δ2-4} mice and the patients with truncated DYX1C1 showed a loss of the outer dynein arms in electron microscopy were observed⁴⁸, suggesting that DYX1C1 is the most likely candidate gene among those identified in this family.

One of the compound heterozygous mutations identified in this study, c.1016dupA p.Asn339fs, was inherited from the father and caused a frameshift, resulting in the truncation of the protein, causing loss of tetratricopeptide repeat (TPR) functional domains. The other mutation, c.249G>C p.Trp83Cys, was inherited from the mother and occurred in another functional domain, CS domain, and was predicted to be pathogenic or deleterious by multiple protein function algorithms such as Polyphen2, LFT, SIFT, MutationTaster, FATHMM,

MetaSVM, MetaLR, and RROVEAN.⁴⁷

However, all PCD families reported in the literature with defective DYX1C1 had truncation mutations located upstream of the mutation identified in this study⁴⁸. Moreover, isoforms of DYX1C1 lacking a portion of the TPR domains have also been reported in human, and in *D. melanogaster*, a functional cilia is observed in the absence of the TPR domain in Dnaaf4/6⁵⁰. In contrast, the variant found in this family lead to truncation in the 8th exon of a total of 9 exons, preserving the first TPR. Therefore, further investigation is necessary to evaluate functions of patients' variants.

3. Lung Airway Organoid from Bronchoscopic Specimens

Five patients who were planned to receive bronchoscopy for their medical purpose were enrolled. (Table 3-2) Bronchoscopic brushing specimens were collected using a protected sheath brush from the right middle lobe bronchus and there was no complication founded. Organoids from all samples were successfully established and stored at -80°C after passage 3 (100% success rate).

Cystic organoids with inner luminal ciliated cells were observed after three weeks of culture (Figure 3-6A) On the H&E staining image and immunofluorescent staining images with acetylated- α -

	Participants (n=5)
Age, year	58 (49 - 70)
Sex, male (%)	2 (40%)
Smoking history, (%)	
Ex-smoker	2 (40%)
Never smoker	3 (60%)
Final diagnosis, (%)	
Early-stage lung cancer	4 (80%)
Amyloidosis	1 (20%)
Bronchiectasis	0 (0%)
COPD, asthma	0 (0%)
Purpose of bronchoscopy, (%)	
Preop evaluation	2 (40%)
EBUS-FNA	2 (40%)
Endobronchial evaluation	1 (20%)

Table 3-2. Characteristics of participants; COPD, chronic obstructive pulmonary disease; EBUS-FNA, endobronchial ultrasound-guided fine-needle aspiration.

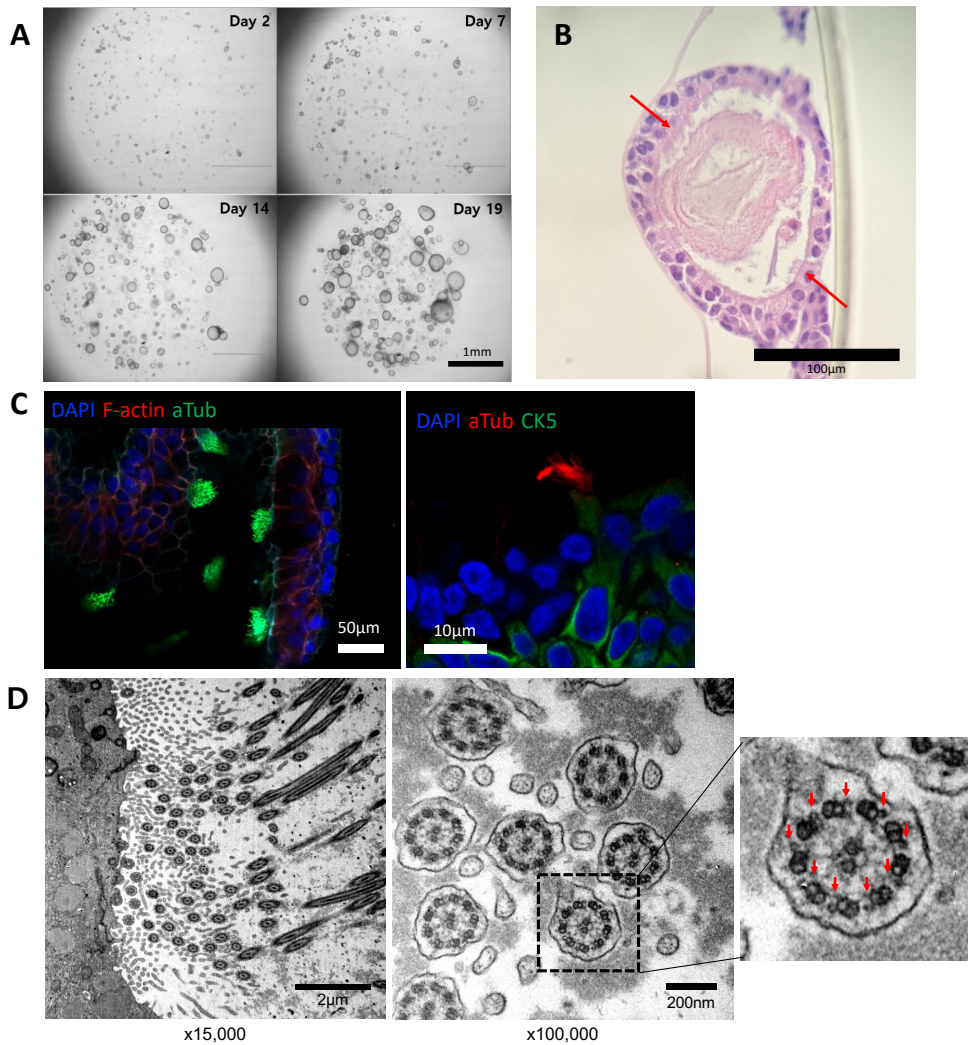


Figure 3-6. Images of established lung airway organoids (A) Time course images of airway organoids for 3 weeks. (B) H&E image of lung airway organoid. Cilia are marked (red arrows) (C) Immunofluorescent images of lung airway organoid. (D) Transmission electron microscopy images of cilia in organoids. Outer dynein arms are marked (red arrows). aTub: acetylated α -tubulin, CK5: keratin 5

tubulin antibody, the mature cilia were confirmed. (Figure 3-6B, C) Transmission electron microscopy image of organoid showed that the cilia had a normal 9+2 structure and normal dynein arms.

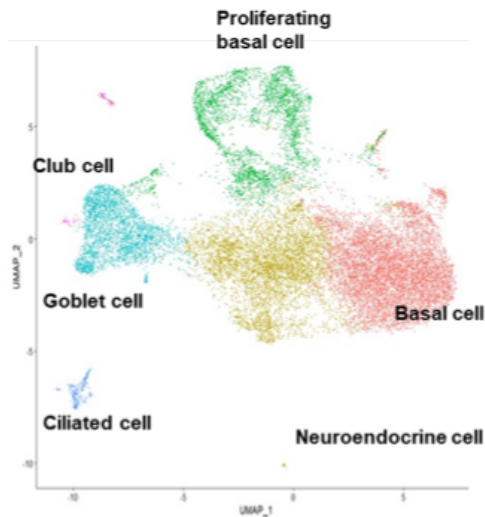


Figure 3-7. UMAP of single cell RNA sequencing data of lung airway organoids.

To investigate whether the cell types and their gene expression patterns of the organoids are similar to those seen in the *in vivo* lung, 10x chromium single-cell RNA sequencing was performed with organoids from all 5 samples. A total of 19,387 cells were captured and 6 distinct clusters with canonical cell markers were identified in UMAP (Figure 3-7); KRT5+ basal cells, KRT5+ Ki67+ proliferating basal cell, FOXJ1+ ciliated cell, MUC5B+ goblet cell, SCGB3A2+ club cell, ASCL1+ neuroendocrine cell, suggesting that organoids closely mimic the characteristics of the lung tissue.

4. CRISPR/Cas9-mediated Lung Organoids Modeling of PCD

To model genetically defective ciliated cells with one of the variants identified in the PCD family (c.1016dupA p.Asn339fs), the indels around the targeted locus were induced using CRISPR/Cas9. Three sgRNAs were designed using CRISPOR⁴² and inserted into the lentiGuide-Puro plasmid (Addgene #52963).⁴³ First, we infected lentiCas9-Blast (Addgene #52962) into a healthy human airway organoid obtained from bronchial brushing and selected them with blasticidin. We then infected each of the lentiGuide-Puro with three sgRNAs and selected with puromycin.

The extent of indel induction was confirmed by T7 endonuclease I assay, and sgRNA #3 was found to be the most efficient, which was used for further functional analysis. (Figure 3-8A) Sanger sequencing was performed to verify the base sequence changes, and it was found that the indels were generated 3 bp next to the protospacer adjacent motif (PAM) site as expected, with an editing efficiency of 12.7%. (Figure 3-8C)

Since this truncation mutation of DYX1C1 is an autosomal recessive mutation, the proportion of cells with actual functional defects might be even lower. This common situation in genome editing is especially important on modeling of ciliary dyskinesia, because a low yield of functional defects on organoids may introduce selection bias as a potential vulnerability.

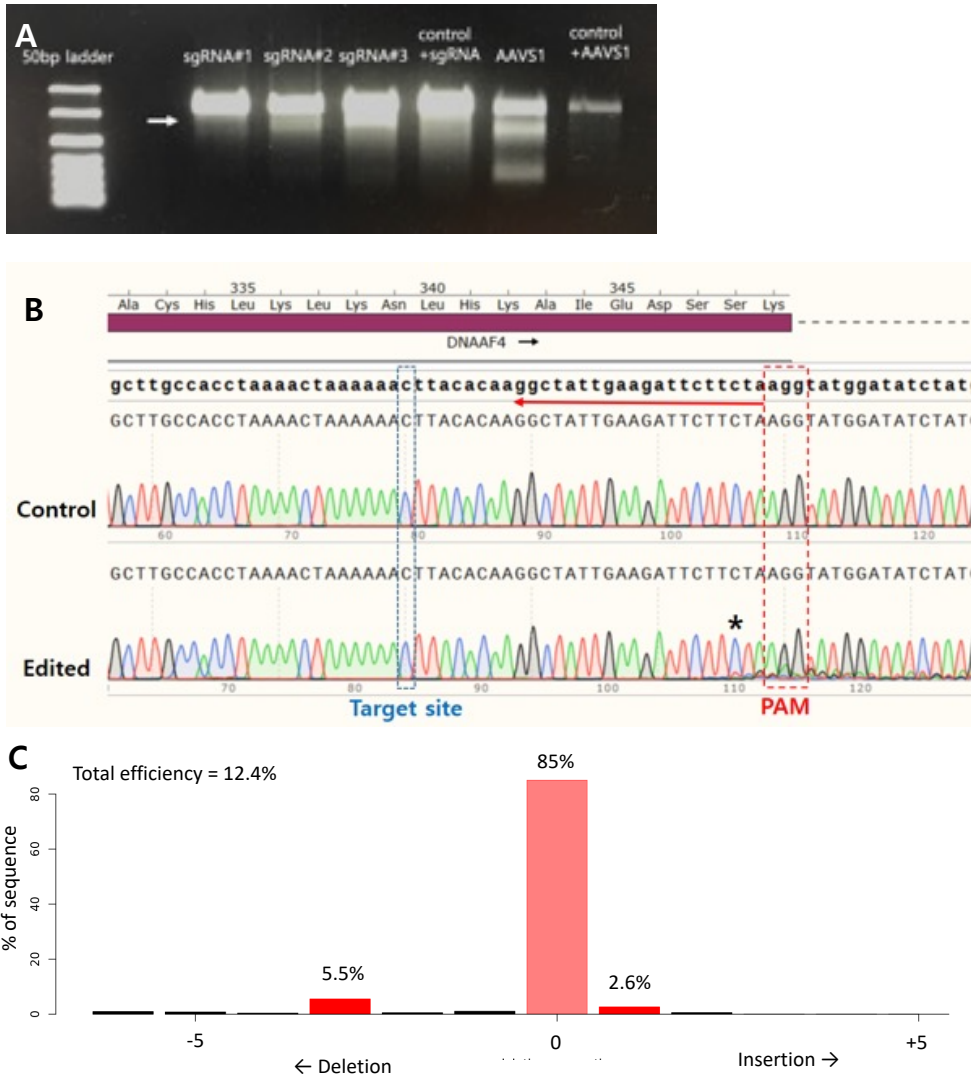


Figure 3-8. Validation of CRISPR/Cas9-mediated gene editing (A) T7 endonuclease I assay for three sgRNA targeting DYX1C1. (B, C) Sanger sequencing of editing with sgRNA#3. The editing targeted position (-3 from PAM) was marked with an asterisk (*). Editing efficiency was calculated with TIDE.

The bright-field image of the DYX1C1-edited organoids were superimposed on its motion-contrast image as described above. The average of the local peaks of the coefficient waveform was measured from individual cilia in three controls and three gene-edited organoids under the same temperature (24°C). The mutant cilia

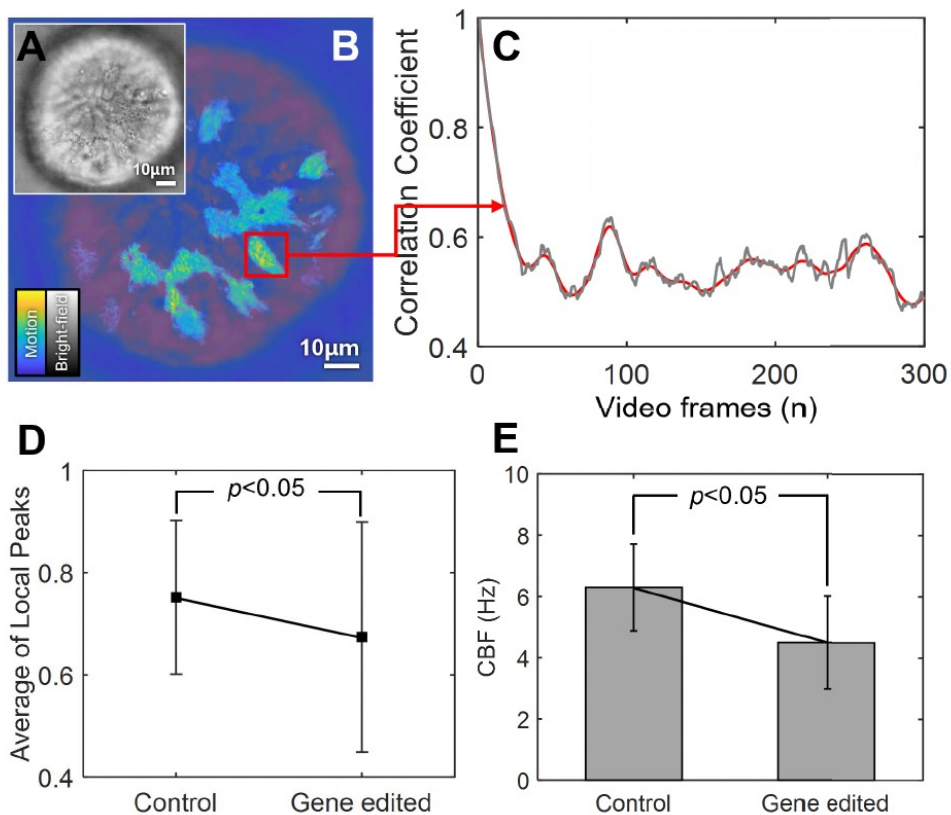


Figure 3-9. CBF of control and edited airway organoids. (A) bright field and (B) motion-contrast images of edited airway organoids. (C) correlation coefficients of ROI (red box in B) (D) Variances of local peaks correlation coefficients on different ROIs (E) Measured CBFs of control and edited airway organoids.

exhibited wider variance in the average scores compared to the control cilia, with a mean value of 0.777 (control) and 0.671 (gene-edited). For cilia with peak averages above the 0.7 threshold, the mean CBF of the mutant cilia was significantly lower than that of the control, indicating that our method can quantitatively detect dysfunctional ciliary motion.

Motion-contrast imaging technique allows for representing the direction of cilia movement as a vector, called optical flow vector, enabling the overall understanding of the movement of multiple cilia within an ROI. These vectors can be seen as metachronal waves within the intra-organoid. Quantitative analysis of metachronal waves

is important for modeling ciliary disease, as foreign substances that enter in the lung are expelled through mucociliary clearance formed by synchronized ciliary motion with mucus. Measuring these bundles of ciliary motion is a labor-intensive task and difficult to examine with single-point analysis, therefore, it is a major advantage of this approach. Interestingly, a significant proportion of cilia in the gene-edited organoid exhibited non-oscillatory correlation profiles with peaks less than 0.6 and also showed irregular optical flow vectors of cilia in organoids.

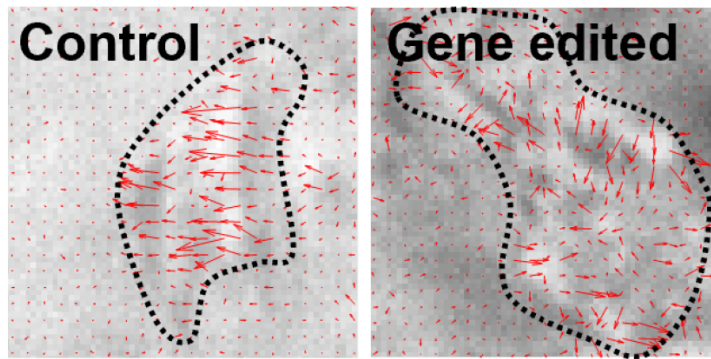


Figure 3-10. Optical flow vectors of organoids (left) metachronal movements of a healthy airway organoid (right) irregular vectors of an edited airway organoid.

Chapter 4. Discussion

Mucociliary clearance is one of the important defense mechanisms of respiratory system. After the secretion of mucus and ions from goblet cells and ionocytes, the foreign particles such as dust, bacteria, and virus particles adhere to them. Then the metachronous movement of cilia then expels these particles back to the external environment. Therefore, ciliary dyskinesia causes recurrent pneumonia, facilitates excessive immune response, and leads to destruction of lung structure.

Despite its importance, measuring ciliary motion has been limited by the drawbacks of conventional CBF analysis, which are highly time-consuming and require extensive operator attention. However, recent advancements in high-speed digital cameras and computerized analysis algorithms have allowed for simpler and faster CBF measurements *in vitro* and *ex vivo*. Despite these improvements, current techniques still present challenges. For instance, the standardized assay currently used for CBF analysis, the Sisson-Ammons video analysis, has several limitations, such as its ability to measure CBFs only on small regions of interest (ROIs), which are subjectively chosen by users and may introduce selection bias.

Selection bias is particularly problematic for samples with variable CBF, such as gene-edited organoids. As mentioned above, gene editing efficiency cannot be 100%, but rather is often on the low side, therefore, edited organoids are found in only a fraction of organoids. In such a situation, CBF values estimated through a

single-point-based FFT approach will be vulnerable to selection bias, as it is difficult to determine the full distribution of CBF.

CRISPR/Cas9 for organoids is the most direct way to validate the function of mutations found in patients. There is a need for a method to accurately measure CBF over a wide area that is fast and simple to use. Furthermore, given the nature of organoids and cilia, a method that is robust to out-of-focusing and overlapping artifacts is needed.

The proposed method offers significant improvements over existing methods. Motion contrast imaging provides cilia that are distinguishable from the background, allowing users to specify ROIs precisely. In addition, the image-based correlation approach automatically determines the effective CBF for individual motor cilia in a user-selected region. It can characterize a wide range of frequency distributions with high sensitivity. In addition, the correlation strategy used is robust to signal blurring due to focus shifts, as the measurements are based on the similarity of image textures, which improves the fidelity of the measurements. In particular, we were able to explore intra- and inter-organoid variability in the organoids and demonstrated its usefulness through the reduced CBF and unsynchronized ciliary motions seen in the edited organoids. The variability was particularly high in the gene-edited organoids, where we also observed a few immobile cilia, which we were able to accurately measure, even though we were concerned that if we measured too few samples, we might miss them or report that the cilia were immobile.

Chapter 5. Conclusion and Perspectives

Despite the critical role of cilia as a defense mechanism in the lung airway, their status as fully differentiated cells have limited genetic perturbation studies. Moreover, there has been no accurate and easy method to analyze the spatial distribution of CBF due to the innate features of ciliary motion. In this doctoral program, (1) I established patient derived organoids and showed that it can be a useful model for cilia study. (2) I and collaborators developed a novel ciliary motion imaging technique to assess spatial distribution of CBF with a minimized bias. (3) I also performed functional validation study of candidate variants with unknown significance identified in a PCD family by using organoids and CRISPR/Cas9 gene editing technique.

Cilia are complex protein complexes, and their interactions are complex, which is why various mutations are constantly being discovered in PCD patients¹⁵. However, there is a lack of functional studies on these mutations. Through the CRISPR/Cas9-mediated organoid model established in this study, it is expected to promote research on PCD-causing genes and cilia-composing proteins in the future, enabling us to explore genotype-phenotype association deeper.

Additionally, the newly developed CBF measurement method enables easy analysis of ciliary movement expressed in various vectors and evaluation of metachronal movement beyond simple CBF values, which can lead to a deeper understanding of various abnormal movements caused by PCD-causing mutations.

Recently, large-scale image analysis based on machine learning has been reported to uncover and utilize hidden features that are easily missed by human observation or traditional measurements alone.⁵¹ Similarly, it is expected that more in-depth analysis of single or bundle ciliary movements will be possible in the future if the cilia motion vector captured by high frequency video and motion-contrast analysis is combined with machine learning techniques.

As the efficiency and delivery techniques of CRISPR/Cas9 system have been improved, now it can not only introduce a variant but also correct the variant⁵². In addition, the method of cultivating on a transplantable mesh in the airway is being developed³¹, bringing us closer to correcting the causes of PCD in patients.

Furthermore, a recent single-cell RNA sequencing comparison between nasal and bronchial epithelial cells suggests that the expression pattern and distribution of ciliated cells, at least, are not significantly different.⁵³ This suggests that nasal brushing, which is even less invasive method than bronchoscopic brushing, would be an optimal sampling method to establish organoids for modeling ciliary function in the future, and indeed one study has reported establishing nasal organoids.³⁰

In addition, patient-derived modeling can be utilized for acquired ciliary dyskinesia caused by infections/inflammations, in addition to inherited ciliary dyskinesia, leading to more helpful research for chronic respiratory patients.

References

- 1 Broaddus, V. C. *et al.* *Murray & Nadel's textbook of respiratory medicine*. Seventh edition. edn, (Elsevier, 2022).
- 2 Weibel, E. R. It takes more than cells to make a good lung. *Am J Respir Crit Care Med* **187**, 342–346 (2013). <https://doi.org/10.1164/rccm.201212-2260OE>
- 3 Dua, K. & ScienceDirect. *Targeting chronic inflammatory lung diseases using advanced drug delivery systems*. 489p. (Academic Press, 2020).
- 4 Lippmann, M., Yeates, D. B. & Albert, R. E. Deposition, retention, and clearance of inhaled particles. *Br J Ind Med* **37**, 337–362 (1980). <https://doi.org/10.1136/oem.37.4.337>
- 5 Lambert, A. R., O'Shaughnessy, P., Tawhai, M. H., Hoffman, E. A. & Lin, C. L. Regional deposition of particles in an image-based airway model: large-eddy simulation and left-right lung ventilation asymmetry. *Aerosol Sci Technol* **45**, 11–25 (2011). <https://doi.org/10.1080/02786826.2010.517578>
- 6 Munkholm, M. & Mortensen, J. Mucociliary clearance: pathophysiological aspects. *Clin Physiol Funct Imaging* **34**, 171–177 (2014). <https://doi.org/10.1111/cpf.12085>
- 7 Wanner, A., Salathe, M. & O'Riordan, T. G. Mucociliary clearance in the airways. *Am J Respir Crit Care Med* **154**, 1868–1902 (1996). <https://doi.org/10.1164/ajrccm.154.6.8970383>
- 8 Bustamante–Marin, X. M. & Ostrowski, L. E. Cilia and Mucociliary Clearance. *Cold Spring Harb Perspect Biol* **9** (2017). <https://doi.org/10.1101/cshperspect.a028241>
- 9 Sanjana, N. E., Shalem, O. & Zhang, F. Improved vectors and genome-wide libraries for CRISPR screening. *Nat Methods* **11**, 783–784 (2014). <https://doi.org/10.1038/nmeth.3047>
- 10 Roberts, A. J., Kon, T., Knight, P. J., Sutoh, K. & Burgess, S. A. Functions and mechanics of dynein motor proteins. *Nat Rev Mol Cell Biol* **14**, 713–726 (2013). <https://doi.org/10.1038/nrm3667>
- 11 Gueron, S. & Levit-Gurevich, K. Energetic considerations of ciliary beating and the advantage of metachronal coordination. *Proc Natl Acad Sci U S A* **96**, 12240–12245 (1999). <https://doi.org/10.1073/pnas.96.22.12240>
- 12 Sleight, M. A. Primary ciliary dyskinesia. *Lancet* **2**, 476 (1981). [https://doi.org/10.1016/s0140-6736\(81\)90811-4](https://doi.org/10.1016/s0140-6736(81)90811-4)
- 13 Horani, A., Ferkol, T. W., Dutcher, S. K. & Brody, S. L. Genetics and biology of primary ciliary dyskinesia. *Paediatr Respir Rev* **18**, 18–24 (2016). <https://doi.org/10.1016/j.prrv.2015.09.001>
- 14 Knowles, M. R., Zariwala, M. & Leigh, M. Primary Ciliary Dyskinesia. *Clin Chest Med* **37**, 449–461 (2016). <https://doi.org/10.1016/j.ccm.2016.04.008>
- 15 Leigh, M. W. *et al.* Primary Ciliary Dyskinesia (PCD): A genetic

- disorder of motile cilia. *Transl Sci Rare Dis* **4**, 51–75 (2019).
<https://doi.org:10.3233/TRD-190036>
- 16 Horani, A. & Ferkol, T. W. Advances in the Genetics of Primary Ciliary Dyskinesia: Clinical Implications. *Chest* **154**, 645–652 (2018).
<https://doi.org:10.1016/j.chest.2018.05.007>
- 17 Chalmers, J. D., Chang, A. B., Chotirmall, S. H., Dhar, R. & McShane, P. J. Bronchiectasis. *Nat Rev Dis Primers* **4**, 45 (2018).
<https://doi.org:10.1038/s41572-018-0042-3>
- 18 Tilley, A. E., Walters, M. S., Shaykhiev, R. & Crystal, R. G. Cilia dysfunction in lung disease. *Annu Rev Physiol* **77**, 379–406 (2015).
<https://doi.org:10.1146/annurev-physiol-021014-071931>
- 19 Yaghi, A. & Dolovich, M. B. Airway Epithelial Cell Cilia and Obstructive Lung Disease. *Cells* **5** (2016).
<https://doi.org:10.3390/cells5040040>
- 20 Boucher, R. C. Muco-Obstructive Lung Diseases. *N Engl J Med* **380**, 1941–1953 (2019). <https://doi.org:10.1056/NEJMra1813799>
- 21 Kim, J., Koo, B. K. & Knoblich, J. A. Human organoids: model systems for human biology and medicine. *Nat Rev Mol Cell Biol* **21**, 571–584 (2020). <https://doi.org:10.1038/s41580-020-0259-3>
- 22 Richter, M. *et al.* From Donor to the Lab: A Fascinating Journey of Primary Cell Lines. *Front Cell Dev Biol* **9**, 711381 (2021).
<https://doi.org:10.3389/fcell.2021.711381>
- 23 Marx, V. Cell-line authentication demystified. *Nat Methods* **11**, 483–488 (2014). <https://doi.org:10.1038/nmeth.2932>
- 24 Neimark, J. Line of attack. *Science* **347**, 938–940 (2015).
<https://doi.org:10.1126/science.347.6225.938>
- 25 Schutgens, F. & Clevers, H. Human Organoids: Tools for Understanding Biology and Treating Diseases. *Annu Rev Pathol* **15**, 211–234 (2020). <https://doi.org:10.1146/annurev-pathmechdis-012419-032611>
- 26 Clevers, H. Modeling Development and Disease with Organoids. *Cell* **165**, 1586–1597 (2016). <https://doi.org:10.1016/j.cell.2016.05.082>
- 27 Lancaster, M. A. & Knoblich, J. A. Organogenesis in a dish: modeling development and disease using organoid technologies. *Science* **345**, 1247125 (2014). <https://doi.org:10.1126/science.1247125>
- 28 Zhao, Z. *et al.* Organoids. *Nat Rev Methods Primers* **2** (2022).
<https://doi.org:10.1038/s43586-022-00174-y>
- 29 Sachs, N. *et al.* Long-term expanding human airway organoids for disease modeling. *EMBO J* **38** (2019).
<https://doi.org:10.15252/emboj.2018100300>
- 30 van der Vaart, J. *et al.* Modelling of primary ciliary dyskinesia using patient-derived airway organoids. *EMBO Rep* **22**, e52058 (2021).
<https://doi.org:10.15252/embr.202052058>
- 31 Vaidyanathan, S. *et al.* High-Efficiency, Selection-free Gene Repair in Airway Stem Cells from Cystic Fibrosis Patients Rescues CFTR Function in Differentiated Epithelia. *Cell Stem Cell* **26**, 161–171 e164 (2020). <https://doi.org:10.1016/j.stem.2019.11.002>
- 32 Youk, J. *et al.* Three-Dimensional Human Alveolar Stem Cell Culture

- Models Reveal Infection Response to SARS-CoV-2. *Cell Stem Cell* **27**, 905–919 e910 (2020). <https://doi.org:10.1016/j.stem.2020.10.004>
- 33 Driehuis, E. & Clevers, H. CRISPR/Cas 9 genome editing and its applications in organoids. *Am J Physiol Gastrointest Liver Physiol* **312**, G257–G265 (2017). <https://doi.org:10.1152/ajpgi.00410.2016>
- 34 Sun, D. *et al.* A functional genetic toolbox for human tissue-derived organoids. *Elife* **10** (2021). <https://doi.org:10.7554/eLife.67886>
- 35 Drost, J. *et al.* Use of CRISPR-modified human stem cell organoids to study the origin of mutational signatures in cancer. *Science* **358**, 234–238 (2017). <https://doi.org:10.1126/science.aao3130>
- 36 Wang, P. *et al.* CRISPR/Cas9-mediated heterozygous knockout of the autism gene CHD8 and characterization of its transcriptional networks in cerebral organoids derived from iPSCs. *Mol Autism* **8**, 11 (2017). <https://doi.org:10.1186/s13229-017-0124-1>
- 37 Artegiani, B. *et al.* Fast and efficient generation of knock-in human organoids using homology-independent CRISPR-Cas9 precision genome editing. *Nat Cell Biol* **22**, 321–331 (2020). <https://doi.org:10.1038/s41556-020-0472-5>
- 38 Gopal, S., Rodrigues, A. L. & Dordick, J. S. Exploiting CRISPR Cas9 in Three-Dimensional Stem Cell Cultures to Model Disease. *Front Bioeng Biotechnol* **8**, 692 (2020). <https://doi.org:10.3389/fbioe.2020.00692>
- 39 Zheng, G. X. *et al.* Massively parallel digital transcriptional profiling of single cells. *Nat Commun* **8**, 14049 (2017). <https://doi.org:10.1038/ncomms14049>
- 40 Fleming, S. J. *et al.* Unsupervised removal of systematic background noise from droplet-based single-cell experiments using <code>CellBender</code>. *bioRxiv*, 791699 (2022). <https://doi.org:10.1101/791699>
- 41 Hao, Y. *et al.* Integrated analysis of multimodal single-cell data. *Cell* **184**, 3573–3587 e3529 (2021). <https://doi.org:10.1016/j.cell.2021.04.048>
- 42 Concordet, J. P. & Haeussler, M. CRISPOR: intuitive guide selection for CRISPR/Cas9 genome editing experiments and screens. *Nucleic Acids Res* **46**, W242–W245 (2018). <https://doi.org:10.1093/nar/gky354>
- 43 Choi, W. J. *et al.* Image Correlation-Based Method to Assess Ciliary Beat Frequency in Human Airway Organoids. *IEEE Transactions on Medical Imaging* **41**, 374–382 (2022). <https://doi.org:10.1109/TMI.2021.3112992>
- 44 Yousefi, S., Zhi, Z. & Wang, R. K. Eigendecomposition-based clutter filtering technique for optical micro-angiography. *IEEE Trans Biomed Eng* **58** (2011). <https://doi.org:10.1109/TBME.2011.2152839>
- 45 Li, H. & Durbin, R. Fast and accurate short read alignment with Burrows-Wheeler transform. *Bioinformatics* **25**, 1754–1760 (2009). <https://doi.org:10.1093/bioinformatics/btp324>
- 46 Poplin, R. *et al.* Scaling accurate genetic variant discovery to tens of

- thousands of samples. *bioRxiv*, 201178 (2018).
<https://doi.org:10.1101/201178>
- 47 Yang, H. & Wang, K. Genomic variant annotation and prioritization
with ANNOVAR and wANNOVAR. *Nat Protoc* **10**, 1556–1566 (2015).
<https://doi.org:10.1038/nprot.2015.105>
- 48 Tarkar, A. *et al.* DYX1C1 is required for axonemal dynein assembly
and ciliary motility. *Nat Genet* **45**, 995–1003 (2013).
<https://doi.org:10.1038/ng.2707>
- 49 Mali, G. R. *et al.* ZMYND10 functions in a chaperone relay during
axonemal dynein assembly. *eLife* **7**, e34389 (2018).
<https://doi.org:10.7554/eLife.34389>
- 50 Lennon, J., Zur Lage, P., von Kriegsheim, A. & Jarman, A. P.
Strongly Truncated Dnaaf4 Plays a Conserved Role in Drosophila
Ciliary Dynein Assembly as Part of an R2TP-Like Co-Chaperone
Complex With Dnaaf6. *Front Genet* **13**, 943197 (2022).
<https://doi.org:10.3389/fgene.2022.943197>
- 51 Schneider, S., Lee, J. H. & Mathis, M. W. Learnable latent
embeddings for joint behavioural and neural analysis. *Nature* **617**,
360–368 (2023). <https://doi.org:10.1038/s41586-023-06031-6>
- 52 Wang, J. Y. & Doudna, J. A. CRISPR technology: A decade of genome
editing is only the beginning. *Science* **379**, eadd8643 (2023).
<https://doi.org:10.1126/science.add8643>
- 53 Deprez, M. *et al.* A Single-Cell Atlas of the Human Healthy Airways.
Am J Respir Crit Care Med **202**, 1636–1645 (2020).
<https://doi.org:10.1164/rccm.201911-2199OC>

국 문 초 록

폐는 외부 공기를 흡입하여 가스 교환을 하는 장기이므로, 필연적으로 외부 물질에 노출된다. 이에 따라, 흡입된 이물질을 제거하기 위한 다양한 방어 기전이 존재한다. 그 중 하나인 핵심적인 세포 소기관인 섬모 (cilium)는 기도의 섬모 세포 (ciliated cell)에 존재하며 서로 동기화된 움직임을 통해 기도에 침착한 이물질을 외부로 밀어낸다. 따라서, 섬모를 구성하거나 조립에 관여하는 유전자 중 하나에 이상이 생기면 유전질환인 일차성 섬모운동장애 (primary ciliary dyskinesia; 이하 PCD)가 발생한다. 또한, 만성 염증이나 반복적인 감염으로 인해 기관지 상피 세포가 손상되면, 다양한 만성 폐질환에서 획득성 섬모운동장애 (acquired ciliary dyskinesia)가 발생하기도 한다. 그럼에도, 여러 가지 이유로 섬모 운동에 대한 연구는 제한적이었다. 우선, 섬모 세포는 분화된 세포이고 분열하지 않기 때문에, 세포주가 따로 존재하지 않아 이를 이용한 연구가 불가능하며 주로 동물 모델이 이용되어왔다. 사람 조직에서 얻은 섬모 세포를 일시적으로 배양하는 일차 세포 배양 (primary cell culture)이 섬모 연구에 널리 쓰이고 있으나, 장기간 배양이 불가능하므로, 유전자 편집 연구에는 적합하지 않다. 또한, 기존 섬모 운동을 측정하는 시간과 노력이 많이 들면서도 편향이 발생하기 쉬우면서 부정확할 때가 있는데, 섬모들은 함께 움직이며 섬모 이미지가 겹쳐보이기 쉽기 때문이다.

박사 학위 기간동안 이를 해결하기 위해 여러 가지 접근을 수행하였다. (1) 호흡기 환자 샘플, 특히 기관지 내시경 브러싱 샘플을 이용하여 사람 폐 오가노이드를 수립하였으며, 섬모 세포를 비롯하여 기관지를 구성하는 세포들이 잘 유도됨을 확인하였다. (2) 공동 연구를 통해 새로운 섬모 운동 측정하는 방법을 개발하였으며, 이를 통해 오가노이드 내 다양하게 존재하는 섬모 운동을 빠르고 정확하게 평가할

수 있게 되었다. (3) PCD 환자 가족의 전장 유전체 염기서열 분석 (whole genome sequencing)에서 발견된 기능을 정확히 알 수 없는 돌연변이를 CRISPR/Cas9 시스템으로 정상 폐 오가노이드에 도입하였고, 이 돌연변이가 섬모 운동 이상을 유발하는 것을 확인하였다.

이번 연구를 통해, CRISPR/Cas9 기반의 사람 폐 오가노이드 유래 섬모 운동 연구 모델이 확립되었다. 이를 통해 PCD 유발하는 다양한 변이들의 기능적 검증이 가능 해졌으며, 향후 돌연변이 교정을 위한 유전자 편집을 위한 기반을 마련하였고, 만성 폐질환으로 인한 획득성 섬모운동장애 연구로의 확장 가능성도 보여주었다.

주요어 : 섬모운동이상, 오가노이드, 유전자 교정, 질환 모델

학 번 : 2020-38357